On-chip interaction-free measurements via the quantum Zeno effect

Xiao-song Ma,[1,2,*] Xiang Guo,[1] Carsten Schuck,[1] King Y. Fong,[1] Liang Jiang,[3] and Hong X. Tang[1,†]

[1]*Department of Electrical Engineering, Yale University, New Haven, Connecticut 06511, USA*

[2]*Institute for Quantum Optics and Quantum Information, Austrian Academy of Science, Vienna, Austria*

[3]*Department of Applied Physics, Yale University, New Haven, Connecticut 06511, USA*

(Received 7 March 2014; revised manuscript received 24 May 2014; published 13 October 2014)

Although interference is a classical-wave phenomenon, the superposition principle, which underlies interference of individual particles, is at the heart of quantum physics. An interaction-free measurement (IFM) harnesses the wave-particle duality of single photons to sense the presence of an object via the modification of the interference pattern, which can be accomplished even if the photon and the object have not interacted with each other. By using the quantum Zeno effect, the efficiency of an IFM can be made arbitrarily close to unity. Here we report an on-chip realization of the IFM based on silicon photonics. We exploit the inherent advantages of the lithographically written waveguides (excellent interferometric phase stability and mode matching) and obtain multipath interference with visibility above 98%. We achieved a normalized IFM efficiency up to 68.2%, which exceeds the 50% limit of the original IFM proposal.

DOI: 10.1103/PhysRevA.90.042109 PACS number(s): 03.65.Ta, 03.67.−a, 42.50.Xa, 42.70.Qs

I. INTRODUCTION

In classical physics, measurement processes require the interaction between the measurement device and the object to be measured. In quantum physics, on the other hand, one can realize so-called interaction-free measurements (IFM), in which a measurement can be made without any physical interaction. The concept of IFMs was first considered by Dicke [1]. Elitzur and Vaidman (EV) extended this idea and proposed a gedanken experiment [2,3]. The goal of this gedanken experiment was to identify the presence of an ultrasensitive bomb (i.e., any interaction with the bomb triggers an explosion) without causing it to explode. To achieve this goal, EV ingeniously proposed a quantum-mechanical method using the wave-particle duality of single photons. They proposed to incorporate the bomb into a Mach-Zehnder interferometer (MZI) to achieve the IFM. The presence of a bomb modifies the optical interferograms of the MZI, even though the photons and the bomb never interacted. By using this method, the ultrasensitive bomb can be found without triggering it. The details of their proposal are the following.

As shown in Fig. 1(a), the relative phase between two arms of the MZI is adjusted to be zero such that any photon entering the MZI from the lower input will go to detector U and no photons will go to detector L due to constructive and destructive interferences, respectively. The probability of photon detection by detector U P(U) is 1, and that by detector L P(L) is 0.

If a bomb is inserted in the upper arm [Fig. 1(b)], the previous destructive interference at detector L is destroyed. The interaction between the photon and the bomb is *not* required. The mere presence of the ultrasensitive bomb destroys the coherence between the path states of the photon and inhibits the interference. Consequently, P(L) will not be zero any more. Any detection event by detector L *unambiguously* indicates the presence of the bomb. Moreover, a single photon is indivisible because of its particle property and cannot be split on a beam splitter [4]. Therefore every single photon detected by L must have propagated through the lower arm of the MZI and hence would not have interacted with the bomb. Every single detection event by L is a successful IFM. The probability of successful IFM P(IFM) equals P(L). The detection events at detector U are inconclusive as they do not tell us whether the bomb is present or not. The input photon can also be absorbed by the bomb, triggering an explosion, with a probability of P(abs). To quantify the performance of an IFM, an efficiency parameter, η_{IFM}, is introduced as the fraction of conclusive measurements which are interaction free [5]:

$$\eta_{\mathrm{IFM}} = \frac{\mathrm{P(L)}}{\mathrm{P(abs)} + \mathrm{P(L)}} = \frac{R_{\mathrm{BS1}} R_{\mathrm{BS2}}}{T_{\mathrm{BS1}} + R_{\mathrm{BS1}} R_{\mathrm{BS2}}}, \tag{1}$$

where R_{BS1} (R_{BS2}) and T_{BS1} (T_{BS2}) are the reflectivity and transmissivity of beam splitter 1 (beam splitter 2). If we use two balanced beam splitters, i.e., $R_{\mathrm{BS1}} = R_{\mathrm{BS2}} = 0.5$, η_{IFM} will be 1/3. EV further showed that by changing the beam splitter's reflectivity one could increase the efficiency of the IFM to 1/2 [shown in Fig. 1(c)].

It is essential to use a pair of complementary beam splitters, i.e., $T_{\mathrm{BS1}} = R_{\mathrm{BS2}}$ and hence $R_{\mathrm{BS1}} = T_{\mathrm{BS2}}$ [Fig. 1(b)]. Given zero relative phase of the MZI, using a pair of complementary beam splitters ensures perfect destructive interference at L when the bomb is absent. This configuration guarantees that when the bomb is present, any detection event in L unambiguously indicates a successful IFM and $\eta_{\mathrm{IFM}} = R_{\mathrm{BS1}}/(1 + R_{\mathrm{BS1}})$.

Note that the visibility between U and L without a bomb is $\frac{[\mathrm{P(U)}-\mathrm{P(L)}]}{[\mathrm{P(U)}+\mathrm{P(L)}]}$ and gives the confidence level of the success of IFM given a detection event by L when the bomb is present. There have been several experimental realizations of EV's IFMs in different physical systems [5–7]. Also, "interaction-free" imaging was reported [8]. Although EV's proposal is elegant, it has two limitations [shown in Fig. 1(c)]: (1) The efficiency of an IFM η_{IFM} has an upper bound of 1/2. (2) When $R = 1$, η_{IFM} is at its maximum, 1/2. But the probability of IFM P(IFM) is arbitrarily close to zero, and the inconclusive measurement P(U) is close to unity. For practical

*Xiaosong.Ma@yale.edu

†Hong.Tang@yale.edu

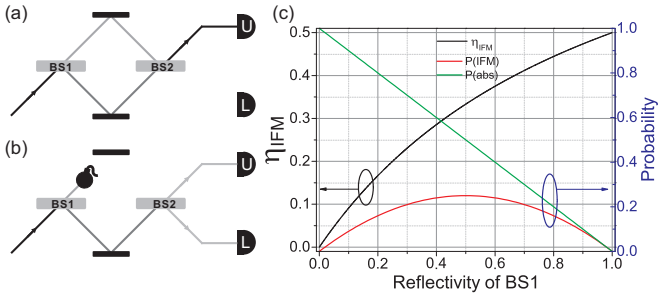

FIG. 1. (Color online) Interaction-free measurement. (a) An optical MZI is formed by two beam splitters (BS1 and BS2) and two mirrors. The MZI is aligned such that all the photons will go to detector U and none will go to detector L. (b) If the bomb is inserted, its presence will destroy the destructive interference at detector L. Each detection event by L indicates the presence of the bomb, and IFM succeeds. (c) The efficiency of the successful IFM η_{IFM}, the probabilities of successful IFM (P(IFM)) and absorption of the photon by the bomb (P(abs)) are shown as black, red (dark gray), and green (light gray) curves, respectively.

IFMs, it is of crucial importance to increase η_{IFM} and P(IFM) at the same time.

In order to enhance the efficiency of an IFM, Kwiat *et al.* combined the discrete form of the quantum Zeno effect [9,10] with IFMs, where one coherently and repeatedly probes a region that might contain the bombs [5,11]. This quantum-Zeno-effect-enabled IFM (QZIFM) in principle allows both η_{IFM} and P(IFM) to approach unity and hence allows the detection of ultrasensitive bombs with an arbitrarily small chance of triggering them (absorbing a photon). The scenario without bombs is depicted in Fig. 2(a). A photon enters the connected Mach-Zehnder interferometers (cMZI), and its path state will *gradually* and *coherently* evolve from the lower half to the upper half of the cMZI. If all the beam splitters' reflectivities fulfill $R = \cos[\pi/(2N)]^2$ (where N is the number of beam splitters), the photon will exit via the upper port of the final beam splitter with certainty after all N stages, i.e., $\mathrm{P(U)} = 1$. The photon has zero probability to exit from the lower port, i.e., $\mathrm{P(L)} = 0$.

As shown in Fig. 2(b), if bombs are inserted into the upper part of the cMZI, the photon's coherent evolution is inhibited, and it will propagate through the lower part of the cMZI with a probability $\mathrm{P(L)} = [\cos^2(\frac{\pi}{2N})]^N$ of being detected by L, whereas this probability is zero when there are no bombs. The probability of the photon being detected by the upper detector U is $\mathrm{P(U)} = [\cos^2(\frac{\pi}{2N})]^{N-1}\sin^2(\frac{\pi}{2N})$. Assuming the cMZI is lossless, the absorption probability is $\mathrm{P(abs)} = 1 - \mathrm{P(L)} - \mathrm{P(U)}$. As shown in Fig. 2(c), one can see both η_{IFM} and P(IFM) increase as N increases and can be arbitrarily close to 1 in the limit of large N. These are the unique advantages of a QZIFM compared to the original IFM.

Since the QZIFM was proposed [5], there have been several endeavors to realize it, including a broadband, discrete method [11]; resonant, continuous methods [12,13]; and a combination of both [14]. The quantum Zeno effect is also essential in certain quantum computation schemes [15], counterfactual quantum computation [16,17], quantum state protection [18], and all-optical switching [19,20]. However, the challenges of the previous demonstration with light [11] are the noise caused by interferometric (subwavelength) instability, despite active stabilization, and imperfect optical elements.

II. REALIZATIONS: INTEGRATED QUANTUM PHOTONICS

Integrated quantum photonics is a promising approach to realize quantum information processing, as it offers interferometric-stable, miniature, and scalable solutions due to its monolithic implementation [21–23]. The silicon-on-insulator (SOI) platform is particularly attractive because (1) it provides good mode confinement due to high refractive index contrast, (2) well-established fabrication techniques allow us to implement complex quantum circuits, (3) it is compatible with superconducting material, which enabled the realization of waveguide-integrated single-photon detectors [24–27], and (4) on-chip quantum interference between single photons [28] and photon-pair sources [29] has been recently realized.

Here we demonstrate discrete quantum-Zeno-effect-enabled IFMs with up to 20 stages on the SOI platform.

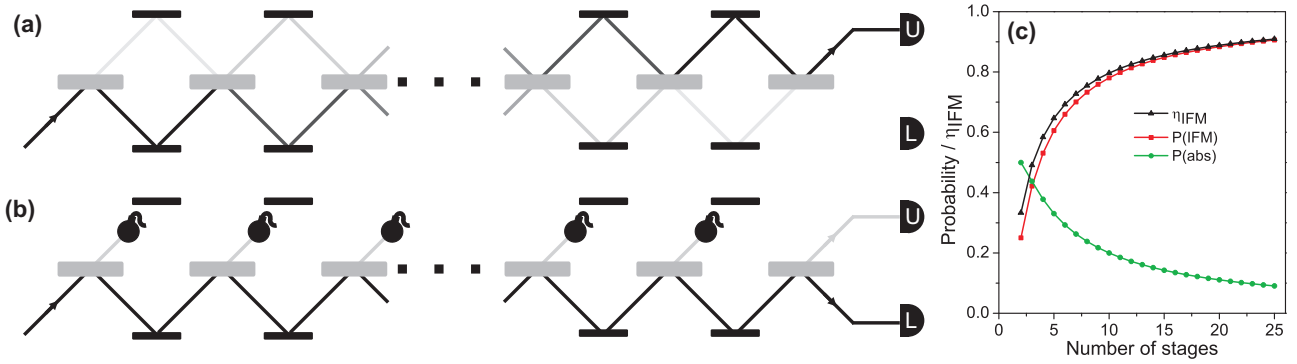

FIG. 2. (Color online) Quantum-Zeno-effect-enabled interaction-free measurement. (a) A photon entering the cMZI from the lower input will coherently and gradually evolve to the upper half of the cMZI and will then be detected by U. (b). If bombs are inserted in the upper arm of the cMZI, the multistage interference is destroyed, and L will detect a large portion of the input photons due to the quantum Zeno effect. (c) By increasing the number of the beam splitters, both η_{IFM} (black triangles) and P(IFM) (red squares) can be made arbitrarily close to 1, and P(abs) (green circles) is reduced to close to 0.

We employ direct-write lithography to realize the circuit conceptually shown in [5] and Fig. 2 to realize a discrete QZIFM without the need of self-stabilized interferometers or active phase stabilization, which greatly enhances the practicality of the implementation of IFM.

Design and fabrication

Waveguides are fabricated on a SOI wafer, which has a 220-nm-thick layer of silicon on top of a 3-μm-thick buried oxide layer that prevents the optical modes from leaking to the substrate. The width of the waveguides is chosen to be 400 nm to ensure (1) single-mode propagation of the transverse-electric (TE) polarized mode, (2) a short coupling length of about 20 μm for various directional couplers, thus achieving small device footprint, and (3) low transmission loss. The gap for evanescent coupling between two waveguides building up a directional coupler is chosen according to the desired beam-splitter reflectivity. The bending radius in our device is chosen to be 10 μm in order to guarantee low bending loss [30]. Waveguides, directional couplers, and grating couplers are defined by electron-beam lithography in hydrogen silsesquioxane resist and are subsequently etched in an inductively coupled chlorine plasma reactive-ion etch.

In our experiment, it is crucial to obtain the desired reflectivities and transmissivities of the directional couplers (DC) accurately because the visibility of the transmission spectra is sensitive to these parameters. In the IFM with a regular two-stage Mach-Zehnder interferometer, we have to ensure the input and output directional couplers have complementary reflectivities, which means that the transmissivity of the output directional coupler T_{out} should equal the reflectivity of the input directional coupler R_{in}. Any mismatch between input reflectivity and output transmissivity will reduce the interference contrast.

In the case of a QZIFM with N directional couplers, the crucial point is to realize directional couplers with the reflectivity $R = \cos[\pi/(2N)]^2$. Only if this condition is fulfilled will Fig. 2(a) be realized (absorbers are absent).

In the presence of absorber waveguides, it is furthermore crucial to make sure that the directional couplers formed by the absorber and the upper arm of the MZI have a reflectivity of zero. Any over- or undercoupling between the absorber and the upper arm of the interferometer will lead to

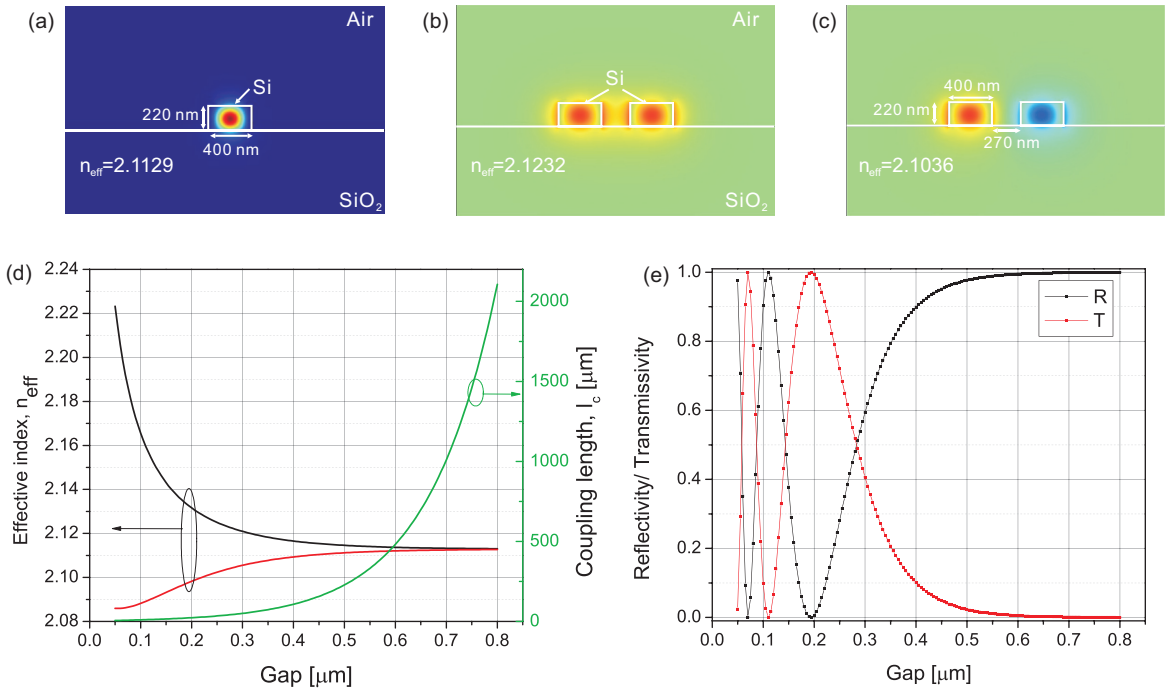

FIG. 3. (Color online) Design of directional couplers. (a) The normalized power distribution of the propagating transverse electric (TE) mode confined by a single Si waveguide that is 400 nm wide and 220 nm thick. The effective refractive index n_{eff} of this mode is about 2.1129. In the coupling region, two waveguides are brought close to each other, and mode hybridization occurs due to the evanescent coupling. Therefore new compound modes become the new eigenmodes. (b) and (c) The simulated TE-like electric-field component E_x of the symmetric and the antisymmetric compound modes. In this simulation, we choose the gap between the two waveguides to be 270 nm. For the symmetric (antisymmetric) mode, the electrical fields distributed in the two silicon waveguides are in (out) of phase, i.e., the relative phase is zero (π). The effective refractive index n_{eff} is about 2.1232 and 2.1036 for the symmetric and antisymmetric modes, respectively. The power and electrical field distributions in (a)–(c) are shown in linear color scale. (d) The effective refractive indexes of these two compound modes as functions of the gap between the two waveguides. The black curve is the effective index of the symmetric mode n_s, and the red curve is that of the antisymmetric mode n_a. See text for details on how the coupling length of these two waveguides l_c can be derived. As we increase the gap, the difference of the effective refractive indexes of these two modes becomes smaller, and hence the coupling length becomes larger. (e) The reflectivity and transmissivity of a directional coupler composed of the above-mentioned waveguides for a design length of 20 μm.

unwanted interference and will lower the confidence level of QZIFM.

In order to have guidance in designing our circuitry, we used a waveguide mode solver (COMSOL) to calculate the effective refractive indexes of the optical modes confined by the waveguide structures. First, we simulate the fundamental TE mode confined by a single Si waveguide that is 400 nm wide and 220 nm thick, as shown in Fig. 3(a), and calculate the effective index and group index of this mode. In the directional coupler region, the two coupling waveguides are close to each other, and mode hybridization occurs due to evanescent couplings [31]. Therefore new compound modes become the new eigenmodes of this coupled waveguides. In Figs. 3(b) and 3(c), we plot the simulated distributions of the TE-like electric-field component E_x of the symmetric and antisymmetric compound modes. In this simulation, we choose the gap between the two waveguides to be 270 nm. For the symmetric (antisymmetric) mode, the electrical fields distributed in the two silicon waveguides are in (out) of phase, i.e., the relative phase is zero (π). In Fig. 3(d), we plot the effective indexes of the symmetric (n_s) and antisymmetric (n_a) modes as a function of the gaps between the waveguides. Based on these effective indexes, we can derive the coupling length of the two straight waveguides via $l_c = \lambda/2(|n_s - n_a|)$. l_c is the length over which the total amount of power is transferred from one waveguide to another.

The grating couplers' design is similar to that in Ref. [32]. Here in order to remove unwanted oscillations from the Fabry-Pérot interferometer formed by the input and output grating couplers, we use an apodized design at the end of each grating coupler.

For device fabrication, we chose a fixed design length for the directional coupler ($l = 20\,\mu$m) and varied the gap between the waveguides. This allowed us to change the effective refractive indexes of the symmetric and antisymmetric modes and hence vary l_c. The incoming and outgoing bend regions increase the coupling length about 2 μm in our case. The transmissivity and reflectivity of the directional couplers are $T = [\sin(\frac{\pi l}{2l_c})]^2$ and $R = [\cos(\frac{\pi l}{2l_c})]^2$, respectively, as shown in Fig. 3(e). Note that in this simulation, we assume the side walls of the waveguides are vertical, which slightly deviates from fabricated devices due to inhomogeneities in dry etching.

Our experimental setup is depicted in Fig. 4. To characterize the device, we use a telecom tunable diode laser (TDL) as the light source. In order to launch light into and collect the output from the QZIFM circuitry under test, a single-mode fiber array with a pitch of 250 μm is used. On the chip, we use grating couplers [32,33] as optical input and output ports.

First, we implement the two-stage IFM depicted in Fig. 1. To characterize the performance of the device, we set the path length of the upper arm to be 100 μm longer than the lower one and measure the transmission spectra with a tunable diode laser and linear photodetectors.

In out MZI devices, we include extra waveguide sections of length $\Delta L = 100\,\mu$m in the upper arms, which act as "highly dispersive" elements in the interferometer [32,34,35]. This allows us to tune the phase by scanning the wavelength of the input and hence to evaluate the performance of the devices by measuring the transmission spectra of the device. In the MZI case, the high-visibility interference in the transmission spectra signals that the first and the second directional couplers are complementary to each other; that is, the reflectivity of the first DC equals the transmissivity of the second DC.

To illustrate this, we consider a simple case of a two-stage interferometer, i.e., a Mach-Zehnder interferometer. The phase difference between the two arms $\Delta\phi$ is given by

$$\Delta\phi = 2\pi\,\Delta L\left(\frac{n_{\text{eff}}}{\lambda}\right), \tag{2}$$

where n_{eff} and λ are the effective refractive index of the propagating mode in a single waveguide and the free-space wavelength, respectively. Since we are interested in the phase shift induced by the wavelength change, we can derive the differential phase shift per unit wavelength $\frac{d(\Delta\phi)}{d\lambda}$:

$$\frac{d(\Delta\phi)}{d\lambda} = 2\pi\,\Delta L\left[\frac{1}{\lambda}\left(\frac{dn_{\text{eff}}}{d\lambda}\right) - \frac{n_{\text{eff}}}{\lambda^2}\right] = -\frac{2\pi\,\Delta L n_g}{\lambda^2}, \tag{3}$$

where n_g is the group index and can be calculated either from experimental data or from simulations. In our case, the group index at 1550 nm is about 4.7 from simulation. To calculate the free spectral range, i.e., the period of the interference pattern, we measure the wavelength difference between the nearest-neighboring interference dips, $\lambda_2 - \lambda_1$, with $\lambda_1 < \lambda_2$. The phase difference between these two wavelength is 2π, and then we have

$$\frac{d(\Delta\phi)}{d\lambda}|_{\lambda=\lambda_2}\lambda_2 - \frac{d(\Delta\phi)}{d\lambda}|_{\lambda=\lambda_1}\lambda_1 = 2\pi. \tag{4}$$

Then by using Eq. (3), we arrive at

$$\left(\frac{1}{\lambda_1} - \frac{1}{\lambda_2}\right) = \frac{1}{n_g\Delta L}. \tag{5}$$

Because λ_1 and λ_2 are close to each other, we here assume that the group index of λ_1 and λ_2 are the same and equal to n_g.

We supply either single photons from very weak coherent light for IFM demonstrations or laser light for device characterizations to port 2. Then the signals are split with a 50:50 splitter. Half of the light is directed to port 1, where it is coupled out into an optical fiber and measured by Det(T). The other half is sent to the QZIFM device. The lower and the upper outputs from the QZIFM device are directed to ports 3 and 5 and are then guided with optical fibers to Det(L) and Det(U), respectively.

We introduced another tapered waveguide as the absorber, or "bomb," which lies close to the upper arm of the interferometer. When the absorber waveguide is positioned 10 μm away from the upper arm of the interferometer, there is negligible coupling between them. Hence this situation represents the case without an absorber. In this case, we experimentally obtain high-contrast transmission spectra at the upper and the lower outputs with above 99.8% interference visibility at the wavelength corresponding to the phase of the multiples of 2π (at a wavelength of 1541.49 nm). The results of a device with 0.852 ± 0.022 reflectivity at the first directional coupler are shown in Fig. 5(a). The reflectivities' uncertainties stem from the uncertainties in the waveguide width control ($\pm$10 nm) during the fabrication process. The upper output's minimum does not go to zero because the directional couplers' reflectivities are not 0.5.

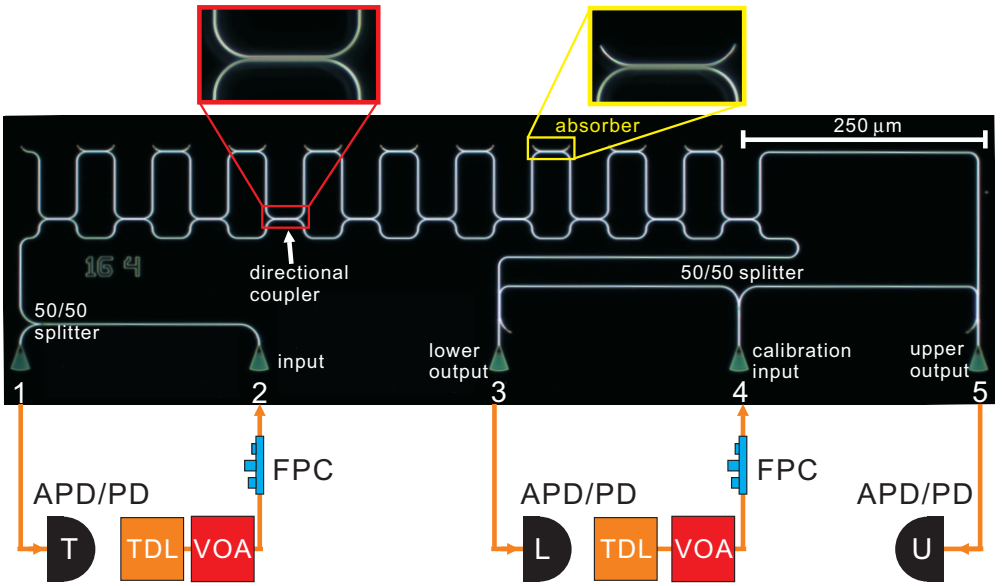

FIG. 4. (Color online) The optical micrograph and schematic setup of a device with 10-stage QZIFM circuitry. There are five grating couplers (GC, labeled by numbers). GC 2 is used as the input. GC 1 couples out half of the total input power, which is measured by detector T. GCs 3 and 5 couple out the lower and upper outputs of the MZI circuit, which are then measured by detectors L and U, respectively. A tunable diode laser (TDL) is used as the light source, and a variable optical attenuator (VOA) is used to attenuate the laser to the single-photon level. A fiber polarization controller (FPC) is used to rotate the polarization of the input light so that it is TE. A set of the same TDL, VOA, and FPC provides a light source to GC 4 for measuring the output coupling differences between GCs 3 and 5. Scale bar is 250 μm.

To demonstrate an IFM, the gap between the absorber and upper arm of the MZI is set such that all the light in the upper arm couples to the absorber waveguide, and hence this absorber is a full absorber. In our case, the gap of a full absorber is about 190 nm. The presence of this full absorber destroys the high-contrast interference. In Fig. 5(b), we show the transmission spectra where the full absorber is present. Note that other than the gap size between absorber and MZI, this device has a nominal design identical to the one shown in Fig. 5(a). It is clearly visible that the interference patterns disappeared. In order to demonstrate an IFM, the laser was attenuated such that the average photon number is about 0.1 per gate and the output photons are measured with single-photon detectors made of InGaAs avalanche photodiodes with a 100-kHz gate.

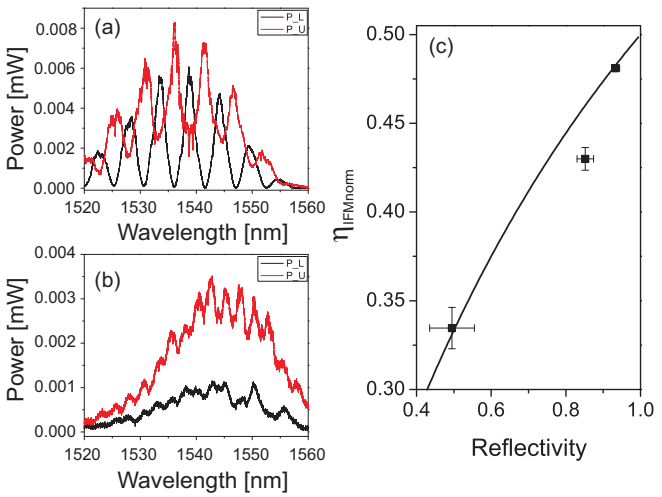

FIG. 5. (Color online) Experimental data of IFM. (a) The transmission spectra of the lower and upper outputs of a device without an absorber [corresponding to Fig. 1(a)]. (b) The transmission spectra with a full absorber present in the upper arm of the interferometer. (c) The result of the two-stage IFM as a function of the reflectivity of the first directional coupler. The black curve is the theoretical prediction as in Fig. 1(c).

We note that in our experiment true single photons and photons from a laser being attenuated to the single-photon level behave similarly because only single-photon interference and linear optics are involved. It is noteworthy that by using photons from a laser being attenuated to the single-photon level, there will be a very small chance (less than 0.05 in our case) that two photons exist simultaneously per gate. These two photons have a small probability to cause the explosion of the bomb as well as the detection events of lower detector. This is similar to using weak coherent laser pulses to implement quantum cryptography [36].

The IFM's efficiencies are derived from the photon counts and are shown in Fig. 5(c). Based on the high-visibility interference, we believe the first DC and the second DC are complementary to each other; that is, the reflectivity of the first DC R_{DC1} equals the transmissivity of the second DC T_{DC2}. We derive the normalized efficiency of the IFM from $\eta_{IFMnorm} = \frac{T_{DC2}}{1+T_{DC2}} = \frac{1}{2+\frac{C_L}{C_U}\frac{a_U}{a_L}}$. C_L, C_U, a_U, and a_L are the single counts and coupling (as well as detecting) efficiencies from the lower output and upper output of the device, respectively. By using the calibration input grating coupler (GC) 4 and a 50:50 splitter, we obtain $\frac{a_L}{a_U}$ and its uncertainties. They are measured at a wavelength of 1541.49 nm. Note that in deriving the normalized efficiency of the IFM, we have factored out the coupling and detecting efficiencies. To improve the efficiency

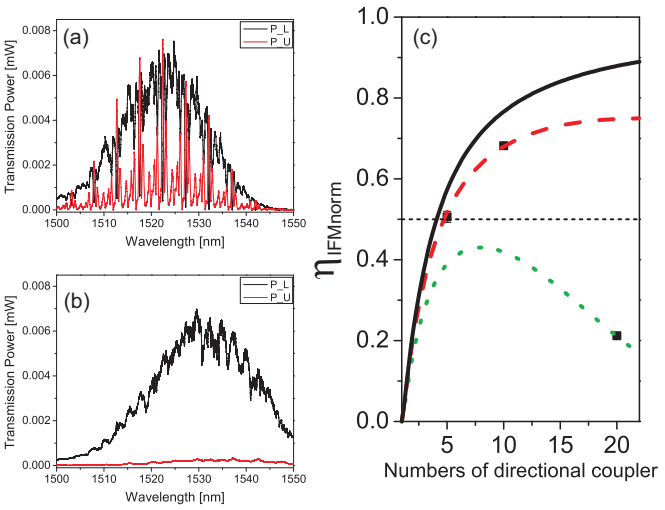

FIG. 6. (Color online) Experimental data of the QZIFM. (a) The transmission spectra of the lower and upper outputs of a ten-stage device without an absorber. (b) The transmission spectra with nine full absorbers present in the upper arm of the interferometer. (c) The results of the 5-, 10-, and 20-stage QZIFMs. The solid black curve is the theoretical prediction of a lossless device. The red dashed and green dotted curves are the predictions with 7.4% and 21.2% loss per stage, respectively. Data for $N = 5$ (measured at the wavelength of 1539.75 nm) and 10 (measured at the wavelength of 1527.25 nm) are in good agreement with the red dashed curve. Data for $N = 20$ (measured at a wavelength of 1538.645 nm) show higher loss and are in agreement with the green curve [37].

of the IFM, it is necessary to include high-efficiency on-chip single-photon detectors [24]. The error bars include both systematic (due to fabrication inhomogeneities) and statistical errors assuming Poissonian statistics.

Next, we employ the quantum Zeno effect to enhance the efficiency of IFM and fabricate devices with multiple connected interferometers as schematically depicted in Fig. 2. A ten-stage QZIFM device is shown in Fig. 4. As mentioned previously, the reflectivity of each directional coupler should be set to $R = \cos[\pi/(2N)]^2$. Only when this condition is fulfilled will the path state of the photon coherently evolve from the lower path to the upper path after N stages, as shown in Fig. 2(a). For $N = 5$, 10, and 20, the reflectivities of each directional coupler are about 0.904, 0.975, and 0.994, respectively.

The measured transmission spectra are shown in Fig. 6(a). Excellent interference with more than 98% visibility has been obtained. Our lithographically defined circuitries provided perfect spatial mode matching and stable phase, which are difficult to achieve with traditional bulk optics, especially for the multistage interferometers. This shows that our system is a very good platform for the development of waveguide quantum optic circuits. Note there are several side peaks with low amplitudes between the main ones with high amplitudes. This is because as the number of directional couplers increases, multipath interference occurs and complicated interference patterns show up.

In the case of QZIFM, we positioned the absorber about 190 nm away from the upper arm of the interferometer, such that all the light is coupled to the absorber from the upper arm. This corresponds to the scenario depicted in Fig. 2(b). In this case, we expect to obtain high output in the lower arm and low output in the upper arm. We present the laser characterization of a QZIFM device with absorbers in Fig. 6(b). We clearly observe that the high-contrast interference disappears. The small modulations visible in Fig. 6(c) originate from the Fabry-Pérot interferometer formed by input and output grating couplers as confirmed by independently tested calibration devices.

Figure 6(c) shows the normalized efficiencies of QZIFM devices with different numbers of directional couplers. We obtained these results by using a strongly attenuated laser as the light source and single-photon detectors [the same as in Fig. 5(c)]. Here we derive the normalized efficiencies of IFM via $\eta_{\mathrm{IFMnorm}} = \frac{C_L}{C_T - C_U \cdot \frac{a_L}{a_U}}$, where C_T, C_L, and C_U are the single-photon counts from GCs 1, 3, and 5. Note that we assume the coupling and detecting efficiencies are the same for the T and L outputs because we use the same fiber and detector to measure C_T and C_L. We obtained η_{IFM} of 0.506 ± 0.014, 0.682 ± 0.008, and 0.212 ± 0.002 for $N = 5$, 10, and 20, respectively. The solid black curve is the theoretical prediction of a lossless device. The red dashed and green dotted curves are the predictions with 7.4% and 21.2% loss per stage, respectively [11,38]. Data for $N = 5$ and 10 are in good agreement with the red dashed curve. We note that for larger N, the device becomes so long that we have to define the lithographic pattern over multiple electron-beam write fields. Hence we attribute the extra loss to the stitching error between waveguides in different write fields [37] and the buildup of the mode-conversion loss in the coupling regions [39].

In conclusion, we report the realization of interaction-free measurement via the quantum Zeno effect on a silicon photonic chip. The future direction would be to further enhance the efficiency of IFM with lower-loss circuitry [30] and on-chip single-photon detectors [24]. Additionally, by using microring resonators made of either Si or SiN, it is possible to further enhance the efficiency of IFM as well as to interrogate the presence of a single absorber via multiple passages, which is similar to the scenario presented in [11] and could be useful for certain practical implementations. Our realizations of the interaction-free measurement via the quantum Zeno effect

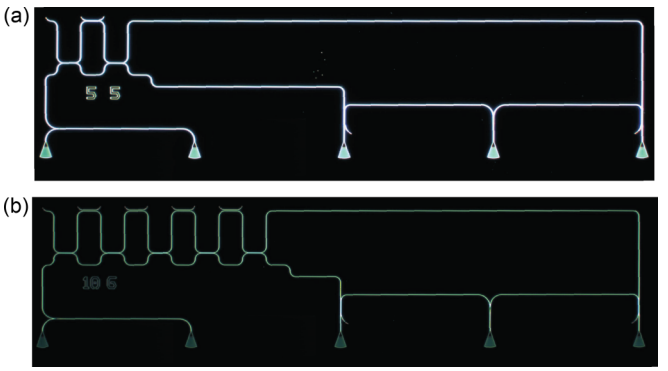

FIG. 7. (Color online) The optical micrographs of (a) a typical two-stage device for IFM and (b) a typical five-stage device for QZIFM.

could be useful in spectroscopic studies of photosensitive materials.

ACKNOWLEDGMENTS

We are grateful to X. Zhang, X. Chi and C. Zou for discussions and A. V. Sergienko for lending us the single-photon detectors. X.S.M. thanks J. Kofler for discussions. X.S.M is supported by a Marie Curie International Outgoing Fellowship within the 7th European Community Framework Programme. C.S. gratefully acknowledges financial support from the Deutsche Forschungsgemeinschaft (SCHU 2871/2-1). L.J. acknowledges support from the Alfred P. Sloan Foundation, the Packard Foundation, AFOSR-MURI, and the DARPA Quiness program. H.X.T. acknowledges support from a Packard Fellowship in Science and Engineering and a CAREER award from the National Science Foundation. We thank Dr. M. Rooks and M. Power for their assistance in device fabrication.

APPENDIX

In this appendix, we first provide a detailed description of the design of the optical waveguides and the directional couplers. Then we present the characterizations of the on-chip interferometers. Finally, we show the data on the quantum-Zeno-effect-enabled interaction-free measurement device with 20 directional couplers.

1. Various devices

Here we show the optical micrographs of a typical two-stage MZI device for IFM in Fig. 7(a) and a five-stage device for QZIFM in Fig. 7(b).

2. The QZIFM device with 20 directional couplers

We have fabricated QZIFM devices with 20 directional couplers, in which we aim to realize directional couplers that each have reflectivity $\cos(\pi/40)^2 = 0.9938$. Based on Fig. 3(e), the gap should be around 0.59 μm in this case.

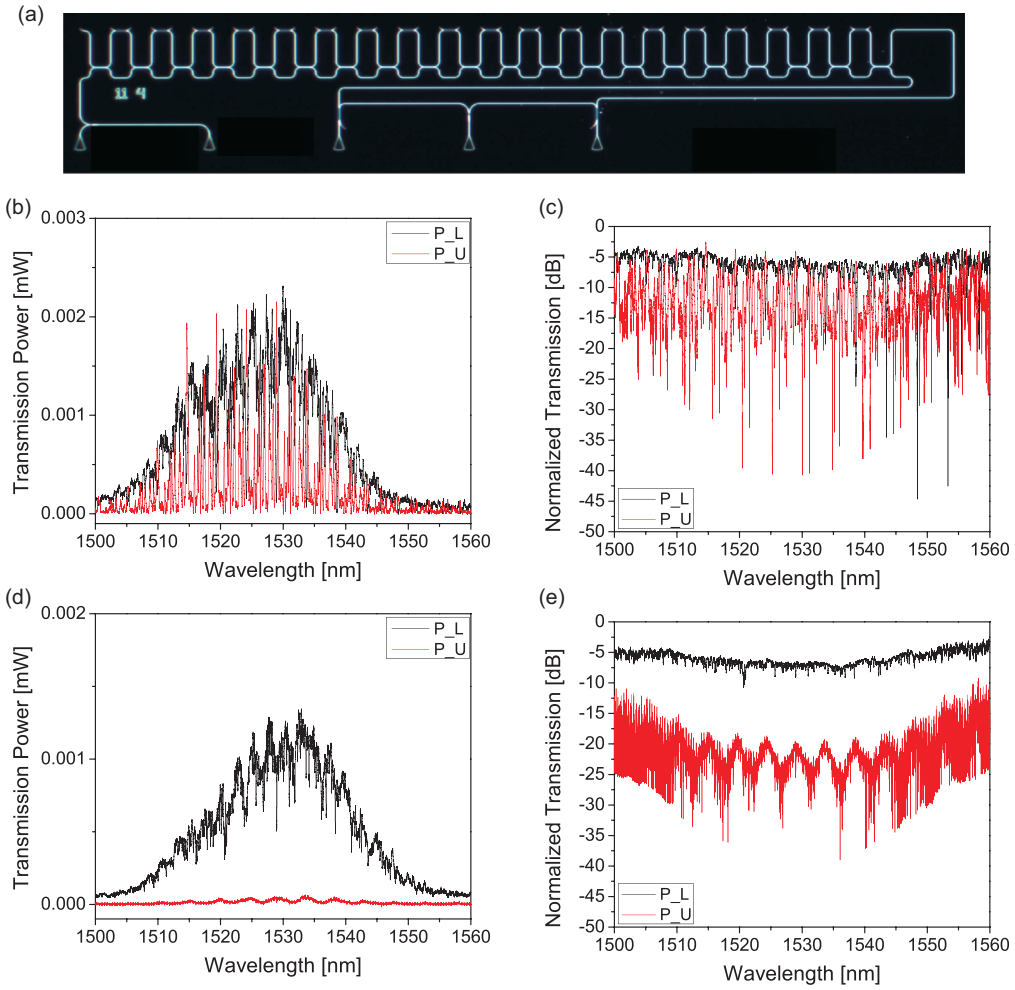

FIG. 8. (Color online) (a) The optical micrograph of a 20-stage device for a QZIFM. (b) The transmission spectra of the lower and upper outputs of a 20-stage device without an absorber, which corresponds to the situation shown in Fig. 2(a). (c) The normalized transmission spectra in logarithm scale. (d) The transmission spectra with 19 full absorbers present in the upper arm of the interferometer. Note that this device has the same design as (b), except the gaps between the absorbers and the upper arm of connected interferometers have changed from 10 μm to 190 nm. (e) The normalized transmission spectra in logarithm scale. It is clear that the interference disappeared, which is the signature of QZIFM.

Experimentally, we found this gap to have a nominal value of 0.532 μm. In Fig. 8(a), we show the optical micrograph of a 20-stage QZIFM device. In Figs. 8(b) and 8(c), we show the transmission spectra of the 20-stage QZIFM device without absorbers in linear and logarithm scales, respectively. In Figs. 8(d) and 8(e), we show the transmission spectra of the device with 19 full absorbers. Comparing these plots with Figs. 8(b) and 8(c), we see that the interference patterns disappear, which is the signature of successful IFM. Note that the loss in the 20-stage QZIFM device is higher than that in the 10-stage QZIFM device, which resulted in lower IFM efficiency [shown in Fig. 5(e)].

[1] R. H. Dicke, Am. J. Phys. **49**, 925 (1981).
[2] A. Elitzur and L. Vaidman, Found. Phys. **23**, 987 (1993).
[3] L. Vaidman, Quantum Opt. **6**, 119 (1994).
[4] P. Grangier, G. Roger, and A. Aspect, Europhys. Lett. **1**, 173 (1986).
[5] P. G. Kwiat, H. Weinfurter, T. Herzog, A. Zeilinger, and M. A. Kasevich, Phys. Rev. Lett. **74**, 4763 (1995).
[6] E. H. du Marchie van Voorthuysen, Am. J. Phys. **64**, 1504 (1996).
[7] M. Hafner and J. Summhammer, Phys. Lett. A **235**, 563 (1997).
[8] A. G. White, J. R. Mitchell, O. Nairz, and P. G. Kwiat, Phys. Rev. A **58**, 605 (1998).
[9] B. Misra and E. C. G. Sudarshan, J. Math. Phys. **18**, 756 (1977).
[10] A. Peres, Am. J. Phys. **48**, 931 (1980).
[11] P. G. Kwiat, A. G. White, J. R. Mitchell, O. Nairz, G. Weihs, H. Weinfurter, and A. Zeilinger, Phys. Rev. Lett. **83**, 4725 (1999).
[12] H. Paul and M. Pavicic, Int. J. Theor. Phys. **35**, 2085 (1996).
[13] T. Tsegaye, E. Goobar, A. Karlsson, G. Björk, M. Y. Loh, and K. H. Lim, Phys. Rev. A **57**, 3987 (1998).
[14] E. W. Streed, J. Mun, M. Boyd, G. K. Campbell, P. Medley, W. Ketterle, and D. E. Pritchard, Phys. Rev. Lett. **97**, 260402 (2006).
[15] J. D. Franson, B. C. Jacobs, and T. B. Pittman, Phys. Rev. A **70**, 062302 (2004).
[16] G. Mitchison and R. Jozsa, Proc. R. Soc. London, Ser. A **457**, 1175 (2001).
[17] O. Hosten, M. T. Rakher, J. T. Barreiro, N. A. Peters, and P. G. Kwiat, Nature (London) **439**, 949 (2006).
[18] G. A. Paz-Silva, A. T. Rezakhani, J. M. Dominy, and D. A. Lidar, Phys. Rev. Lett. **108**, 080501 (2012).
[19] Y. H. Wen, O. Kuzucu, M. Fridman, A. L. Gaeta, L.-W. Luo, and M. Lipson, Phys. Rev. Lett. **108**, 223907 (2012).
[20] K. T. McCusker, Y.-P. Huang, A. S. Kowligy, and P. Kumar, Phys. Rev. Lett. **110**, 240403 (2013).
[21] B. J. Metcalf *et al.*, Nat. Commun. **4**, 1356 (2013).
[22] M. G. Thompson, A. Politi, J. C. F. Matthews, and J. L. O'Brien, IET Circuits Devices Syst. **5**, 94 (2011).
[23] J. L. O'Brien, A. Furusawa, and J. Vuckovic, Nat. Photonucs **3**, 687 (2009).
[24] W. Pernice, C. Schuck, O. Minaeva, M. Li, G. N. Goltsman, A. V. Sergienko, and H. X. Tang, Nat. Commun. **3**, 1325 (2012).
[25] C. Schuck, W. Pernice, and H. Tang, Appl. Phys. Lett. **102**, 051101 (2013).
[26] C. Schuck, W. Pernice, X. Ma, and H. Tang, Appl. Phys. Lett. **102**, 191104 (2013).
[27] C. Schuck, W. Pernice, and H. Tang, Sci. Rep. **3**, 1893 (2013).
[28] X. Xu *et al.*, Opt. Express **21**, 5014 (2013).
[29] J. W. Silverstone *et al.*, Nat. Photonics **8**, 104 (2014).
[30] Y. Vlasov and S. McNab, Opt. Express **12**, 1622 (2004).
[31] B. E. Little and W. P. Huang, Prog. Electromagn. Res. **10**, 217 (1995).
[32] M. Li, W. Pernice, C. Xiong, T. Baehr-Jones, M. Hochberg, and H. X. Tang, Nature (London) **456**, 480 (2008).
[33] D. Taillaert, P. Bienstman, and R. Baets, Opt. Lett. **29**, 2749 (2004).
[34] Y. A. Vlasov, M. O'Boyle, H. F. Hamann, and S. J. McNab, Nature (London) **438**, 65 (2005).
[35] E. Dulkeith, F. Xia, L. Schares, W. M. J. Green, and Y. A. Vlasov, Opt. Express **14**, 3853 (2006).
[36] N. Gisin, G. Ribordy, W. Tittel, and H. Zbinden, Rev. Mod. Phys. **74**, 145 (2002).
[37] See the appendix for a detailed description of the design of the directional couplers, the characterizations of the on-chip interferometers, and the data for the quantum-Zeno-effect-enabled interaction-free measurement device with 20 directional couplers.
[38] P. G. Kwiat, Phys. Scr. T **76**, 115 (1998).
[39] F. Xia, L. Sekaric, and Y. A. Vlasov, Opt. Express **14**, 3872 (2006).